Interferometric droplet imaging for *in situ* aerosol characterization in an inductively coupled plasma†

Kaveh Jorabchi, Ryan G. Brennan, Jonathan A. Levine and Akbar Montaser*

Received 27th March 2006, Accepted 23rd May 2006
First published as an Advance Article on the web 5th June 2006
DOI: 10.1039/b604403d

Size, velocity and evaporation rate of droplets in an Ar inductively coupled plasma (ICP) are simultaneously measured for the first time using a novel laser based imaging technique. In interferometric droplet imaging (IDI), an interference pattern created by the reflected and refracted rays from a droplet are collected in an out-of-focus image. The droplet diameter is determined by counting the number of fringes in the collected interference pattern. Combination of IDI and particle tracking velocimetry (PTV) provides the capability of monitoring droplet properties during the journey inside ICP. Using a demountable-direct injection high efficiency nebulizer, droplets in the range of 3–30 μm in diameter traveling at 15–70 m s^{-1} are observed in the analytical zone of the ICP. The upper velocity threshold for surviving droplets is determined by the nebulizer gas flow rate, whereas the lower threshold is mainly influenced by thermal expansion of the plasma gas. Droplet evaporation rates (0.26–0.36 mm^2 s^{-1}) are in good agreement with other reports and theoretical simulations for droplets in a 3000 K Ar environment.

1. Introduction

The analytical performance of inductively coupled plasma (ICP) spectrometries[1,2] is closely related to the efficiency of sample introduction systems. For liquid samples, an optimum sample introduction device must ideally convert the liquid stream to a mist of monodisperse droplets for the efficient transport of the entire aerosol to the axial channel of the ICP. Several methods have been used to explore the generation and properties of the aerosol for flame and ICP spectrometries,[3–15] but only a few have been applied to *in situ* characterization of the droplets inside plasmas.[16–24] The *in situ* approach is particularly important to discern the optimum aerosol properties (spatial distribution, size, and velocity) for the complete evaporation of the droplets inside ICP. The incompletely desolvated droplets serve as local heat sinks leading to cooling effects, reduced sensitivity, and elevated noise levels.[16,18,19] Moreover, *in situ* experimental studies are useful in evaluating the accuracy of theoretical models for predicting droplet evaporation and transport in ICPs.[25–29]

Thus far, two approaches have been used to examine droplet properties inside ICPs: (1) indirect method, and (2) direct measurements. In the indirect method, the number of surviving droplets in the analytical zone of the plasma is counted using laser light scattering followed by the comparison of the result with absolute counts of the droplets before interaction with the plasma.[16] This approach has led to the estimation that droplets having a diameter of 10 μm or smaller undergo complete desolvation when a conventional nebulizer-spray chamber combination is used. In the direct approach, droplet properties such as size and velocity are measured during their journey inside the plasma. The data can then be used to calculate the evaporation rate and consequently the droplet diameter and velocity thresholds for complete desolvation.

Generally, optical methods are preferred for their non-intrusive nature in direct measurements. However, the small size of the droplets encountered in ICP spectrometries and the strong emission from the plasma create difficulties in conducting optical characterization. In one study, a phase Doppler particle analyzer (PDPA) was used in conjunction with morphology dependent resonances of Mie scattering to measure the size change inside the plasma for droplets created by a monodisperse dried microparticulate injector (MDMI).[24] An evaporation rate of 0.28 mm^2 s^{-1} was calculated in a 1 kW ICP, resulting in a maximum size threshold of 20 μm for complete desolvation with an assumption that the droplets travel at the gas velocity. This method, however, is not applicable to the aerosol from common sample introduction devices where a polydisperse aerosol is generated. In addition, droplets may travel at significantly different velocities than the gas flow, especially for direct injection devices.[23]

In another study using MDMI, the appearance of sodium atomic emission was used to mark the complete desolvation instance of the known size droplets for a range of NaCl concentrations.[21] The decrease in the droplet desolvation time at higher NaCl concentrations was attributed to the lower amount of solvent present in the droplets. The evaporation times for droplets of variable NaCl content were then related to the final particle diameter, estimated by the density of the solid particle (NaCl), resulting in an evaporation rate of 0.38 mm^2 s^{-1} for a 1 kW ICP.[21] In this study, MDMI was assumed to produce constant size droplets at variable matrix

Department of Chemistry, The George Washington University, Washington, DC 20052, USA. E-mail: montaser@gwu.edu; Fax: +1 202 994 5873; Tel: +1 202 994 6480
† Invited talk presented at the 2006 Winter Conference on Plasma Spectrochemistry, Tucson, AZ, USA, January 8–14, 2006.

concentrations (up to 1000 mg L^{-1}), and the particle evaporation time to produce a detectable atomic emission line was neglected in comparison to the droplet desolvation time.

Recently, we introduced an imaging technique to visualize and measure the velocity of the incompletely desolvated droplets inside ICP.[23] This approach, however, can not provide information regarding the size of the surviving droplets. In the current report, interferometric droplet imaging (IDI) is investigated for the first time for direct and simultaneous measurements of size, velocity, and evaporation rate of the droplets in the analytical zone of an ICP. The IDI method has been applied to characterize fuel sprays and droplets in combustion flames, however, its application in ICP is challenging due to the small size of the droplets and intense background emission from the plasma.[30–37]

The IDI method is applicable to any sample introduction device, yet our studies are focused on a demountable direct injection high efficiency nebulizer (d-DIHEN),[38] partly because the aerosol from direct injection devices is coarser than that of conventional nebulizer-spray chamber arrangements, resulting in deterioration of plasma properties and greater levels of matrix effects.[39,40] *In situ* measurements of aerosol properties can reveal causes of matrix effects and the trends in spatial distribution of analyte signal and plasma properties.[23]

1.1. Interferometric droplet imaging

When a droplet is illuminated by a laser sheet, a portion of light is reflected from the gas–droplet interface. The light also passes through the droplet and is refracted at the second droplet–gas interface. The reflected and refracted rays may be collected by a lens to form two glare points within the droplet perimeters (dashed circle, Fig. 1) on the focus image plane. The size of a large droplet can be determined by measuring the distance between the two glare points, assuming a high resolution digital camera is used along with a high magnification lens. As the droplet size becomes smaller (<50 μm diameter), the two glare points merge, preventing drop sizing with this method. Interferometric droplet imaging can be utilized to overcome this obstacle as described below.

By adjusting the position of the image plane (or the distance between the droplet and the lens) a diameter-dependent interference pattern is formed in an out-of-focus image (Fig. 1). This interference pattern can be explained by considering the optical path lengths (OPL) of the reflected and refracted rays (Fig. 2). The light rays reaching a small area on the camera lens from the two sides of the droplet may be considered parallel because of far field conditions (large droplet–lens distance, compared to the droplet diameter). Before interaction with the droplet, the rays are parallel and in-phase due to the use of a laser light source. However, the different optical path lengths create a phase difference between the two rays when they reach a small area on the lens. This phase difference between the two rays depends on the view angle (θ), resulting in angular fringe formation.

To determine the angle between the fringes ($\delta\theta$), the optical path length difference between the two rays (ΔOPL(θ)) is calculated. The resulting function is then differentiated and is made equivalent to one wavelength (λ):

$$\mathrm{d}\Delta\mathrm{OPL}(\theta) = \lambda \qquad (1)$$

This mathematical procedure assumes that a change of one wavelength in ΔOPL(θ) (equivalent to a phase shift of 2π) occurs when one moves from a particular fringe to the adjacent one. eqn (2) shows the results of the calculations for $\delta\theta$:[31]

$$\delta\theta = \frac{2\lambda}{d\left(\cos(\theta/2) + \frac{n\sin(\theta/2)}{\sqrt{1+n^2-2\cos(\theta/2)}}\right)} \qquad (2)$$

where d is droplet diameter, and n is the refractive index of the droplet. Because of the far field conditions, an average θ, corresponding to the angle between the camera optical axis and laser propagation direction (Fig. 1), may be used in the calculations. The number of fringes (N) observed in an out-of-focus image depends on the collection angle (α, Fig. 1) as given

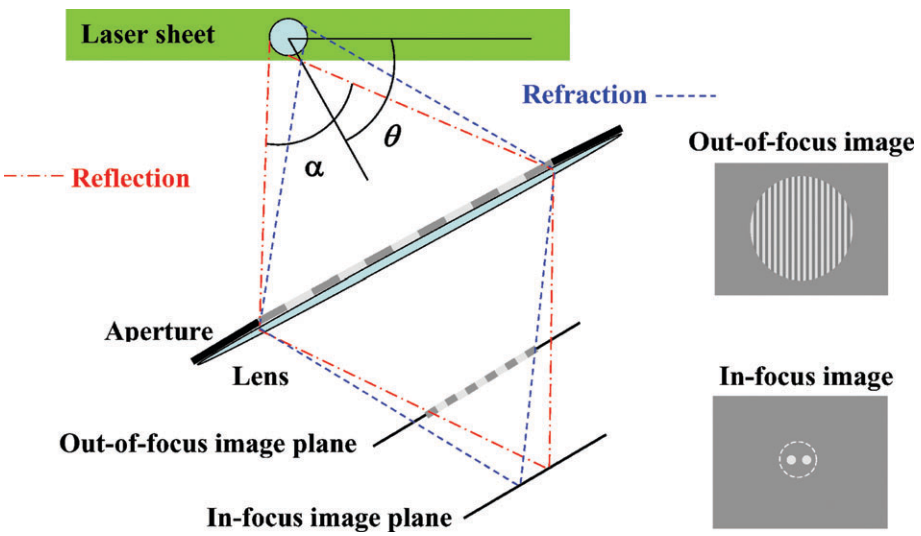

Fig. 1 Formation of glare points in an in-focus image; and fringe formation in an out-of-focus image by interference of refracted and reflected rays. The laser sheet plane is perpendicular to the plan of the paper. The dashed circle in the in-focus image represents the droplet perimeter.

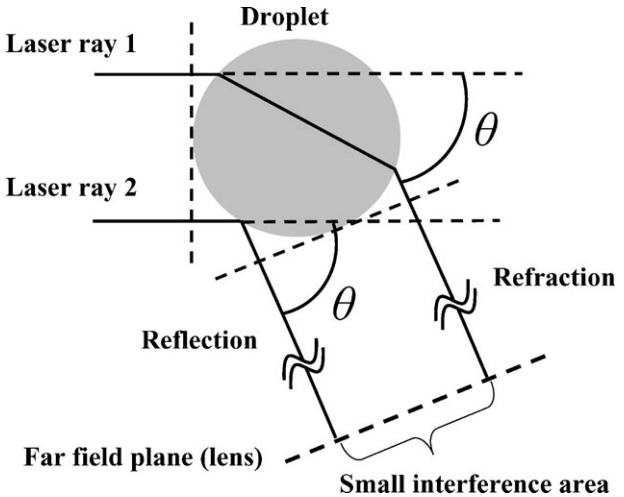

Fig. 2 Optical path lengths of reflected and refracted rays collected on a far field plane (lens). The small area on the lens where constructive/destructive interference occurs is illustrated with a bracket.

by eqn (3):

$$N = \frac{\alpha}{\delta\theta} \tag{3}$$

Combining eqn (2) and (3) results in eqn (4), illustrating that the size of the droplet is linearly proportional to the number of fringes in the out-of-focus image:

$$d = \frac{2\lambda N}{\alpha\left(\cos(\theta/2) + \frac{n\sin(\theta/2)}{\sqrt{1+n^2-2n\cos(\theta/2)}}\right)} \tag{4}$$

Therefore, the droplet diameters can be calculated from the number of fringes in the image, knowing the instrumental parameters (θ and α). For smaller droplets, the angular fringe spacing becomes larger, requiring a larger collection angle for the size determination. The smallest size that could be measured by this method corresponds to the collection of one fringe and depends on instrumental parameters, mainly the collection angle and laser light wavelength. Note that the image size mainly depends on the distance between the lens and the droplet, thus, bearing no information regarding the actual size of the droplet. Moreover, this method faces some limitations for dense aerosol characterization where the droplet images overlap and fringe counting is not feasible. However, other optical setups may be utilized to create an off-focus image only in one dimension, reducing the overlap probability and increasing the applicable particle density limit.[32–34]

2. Experimental

2.1. ICP operating conditions

The instrumentation and operating conditions for the ICP and sample introduction system are summarized in Table 1. The ICP is operated at a power of 1400 W and d-DIHEN is utilized for sample introduction using distilled-deionized water (18.3 MΩ cm resistivity).

2.2. Imaging instrumentation

A schematic diagram of the experimental setup (SprayMaster, LaVision Inc., Ypsilanti, MI) is shown in Fig. 3. The setup consists of a dual cavity frequency-doubled Nd:YAG pulsed laser (15 mJ pulse^{-1}, 7 ns pulse duration, 532 nm, 15 Hz repetition rate, New Wave Research Inc., Fremont, CA) with its set of cylindrical lenses to generate a $\sim$1 mm thick laser sheet. The interference pattern is recorded by an electronically shuttered inline-transfer charge coupled detector (CCD) (1376 × 1040 pixels, 6.45 μm × 6.45 μm, 12 bit digital output, 10 frames s^{-1} rate, LaVision Inc., Ypsilanti, MI) accompanied by a 100 mm focal length lens (T* 100 mm f/2.8 Makro-Planar, 35.4 mm lens diameter, Carl Zeiss Inc., Oberkochen, Germany) at unity magnification positioned face-on (parallel) to the laser sheet (θ = 90°). The laser and the camera are controlled and synchronized *via* software (Version 6, DaVis, LaVision Inc., Ypsilanti, MI) on a personal computer using a programmable timing unit (2 input triggers, 16 output channels). Note that the view window is a rectangle of 8.4 mm × 6.4 mm placed at 7 mm downstream of the load coil at the center of the plasma (Fig. 3). This region corresponds to the analytical zone of the ICP for emission spectroscopy and mass spectrometry.

Reduction of the background light in the images is effected by a narrow band-pass notch filter (532 ± 10 nm, CVI Laser, Putnam, CT) placed in the optical path to selectively transmit the laser light and block the intense continuum and line emission from the argon plasma. A 28.5 mm diameter circular aperture (made in the lab from a 0.5 mm thick black paper sheet) used in front of the notch filter creates a collection angle (α) of 12.2°. Note that the camera lens is operated at widest aperture setting (f/2.8) to avoid any light blockage by the internal diaphragm of the lens.

Using the instrumental parameters noted above and a refractive index of 1.333 (water droplets in air at 298 K), a proportionality constant (slope) of 2.95 μm is calculated for the relationship between the droplet diameter and number of fringes (eqn (4)). Therefore, the smallest measurable droplet diameter with the current setup is 3 μm, corresponding to appearance of a single fringe in the image. The average size of the out-of-focus droplet image is about 160 pixels, leading to a maximum discernable fringe number of 80, according to Nyquist theorem, thus, limiting the maximum measurable droplet size to 240 μm with the current setup. Note that this is an overestimation of the upper limit because the pixels have a finite size across which the intensity will be averaged, leading to loss of spatial information. Nevertheless, the dynamic range of the measurements is large enough to cover the droplet sizes encountered in ICP spectrometries (< 50 μm).

2.3. Fringe counting

For accurate determination of the number of fringes, a horizontal intensity profile across the diameter of each droplet is extracted from the image (Fig. 4A). The resulting function (Fig. 4B) is subjected to fast Fourier transform (FFT) using a statistical data analysis software (Origin 6, OriginLab Corporation, Northampton, MA) followed by identification of three most intense peaks in the power spectrum (Fig. 4C). An

Table 1 Operating conditions for the ICP instrument and sample introduction system

ICP instrument	
RF generator	PE-Sciex Elan 5000 (Perkin-Elmer Corporation, Norwalk, CT)
RF power/W	1400
Nominal frequency/MHz	40
RF generator type	Free-running
Induction coil circuitry	3 turn coil, Electronically balanced, PlasmaLok®
Torch dimensions/mm	Outer tube od = 20; outer tube id = 18; intermediate tube od = 16; intermediate tube id = 14
Nebulizer/injector tip position	5 mm upstream the intermediate tube
Outer gas flow rate/L min^{-1}	15, controlled by a Matheson gas flow meter (Model MFMR-0800-AA; 605, Matheson Gas Products, East Rutherford, NJ)
Intermediate gas flow rate/L min^{-1}	1, controlled by a Matheson gas flow meter (Model MFMR-0800-AA; 603, Matheson Gas Products)
Sample introduction system	
Nebulizer	Demountable DIHEN (nozzle id = 175 μm; Capillary: 75 μm id, 150 μm od)
Nebulizer gas flow rate/L min^{-1}	0.15–0.2
Solution uptake rate/μL min^{-1}	85, controlled by a syringe pump (Model KDS100, KD Scientific, New Hope, PA) and PEEK pump tubing (0.010 in id; Upchurch Scientific, Oak Harbor, WA)

adjusted Gaussian fitting is then utilized to calculate the wave number corresponding to the main fringe pattern in the image based on the following equations:[33]

$$\Delta k = \frac{1}{2}\frac{\log\left(\frac{P_{k-1}}{P_k}\right) - \log\left(\frac{P_{k+1}}{P_k}\right)}{\log\left(\frac{P_{k-1}}{P_k}\right) + \log\left(\frac{P_{k+1}}{P_k}\right)} \quad (5)$$

$$f^* = f\,(k + 0.9169\Delta k + 0.3326\Delta k^3) \quad (6)$$

where k is the integer index of the wavenumber for the most intense peak in the discrete FFT power spectrum, P_k is the corresponding power, and f is the fundamental wavenumber (frequency) of FFT. This fitting results in an adjusted wave number (f^*) which is accurate to the 0.2% of the fundamental wavenumber of the FFT.[33] The number of fringes is finally calculated by multiplying the adjusted wavenumber by the droplet image diameter in pixels. This approach leads to an error of less than 5% for the droplets smaller than 50 μm in diameter, normally encountered in ICP spectrometries.[37]

2.4. Velocity measurements

Velocity measurements are conducted using particle tracking velocimetry (PTV) technique. In this method, the camera shutter is kept open and two laser shots are fired with a known time lag (Δt = 45 μs), resulting in a double exposure image in which the position of the moving droplet is recorded at two instances. The distance traveled (Δx) corresponds to the distance between the centers of the conjugate droplets in the out-of-focus image, and is measured by calibrating the camera using a target with vertical lines of 0.1 mm apart (1 mm = 163 pixels). The axial velocity is subsequently calculated by $\Delta x/\Delta t$. A typical calibrated double exposure image for simultaneous size and velocity measurements is shown in Fig. 5. The image consists of 5 droplet pairs with different sizes (number of

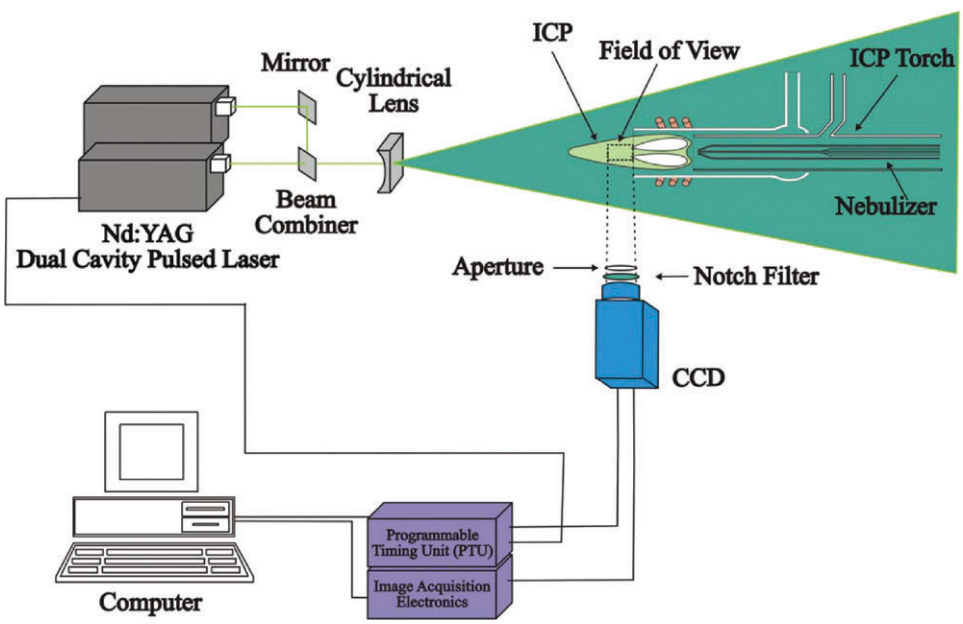

Fig. 3 Instrumental setup for interferometric droplet imaging. Note that the field of view is a rectangle (8.4 mm × 6.4 mm) placed at 7 mm downstream of the load coil at the center of the plasma.

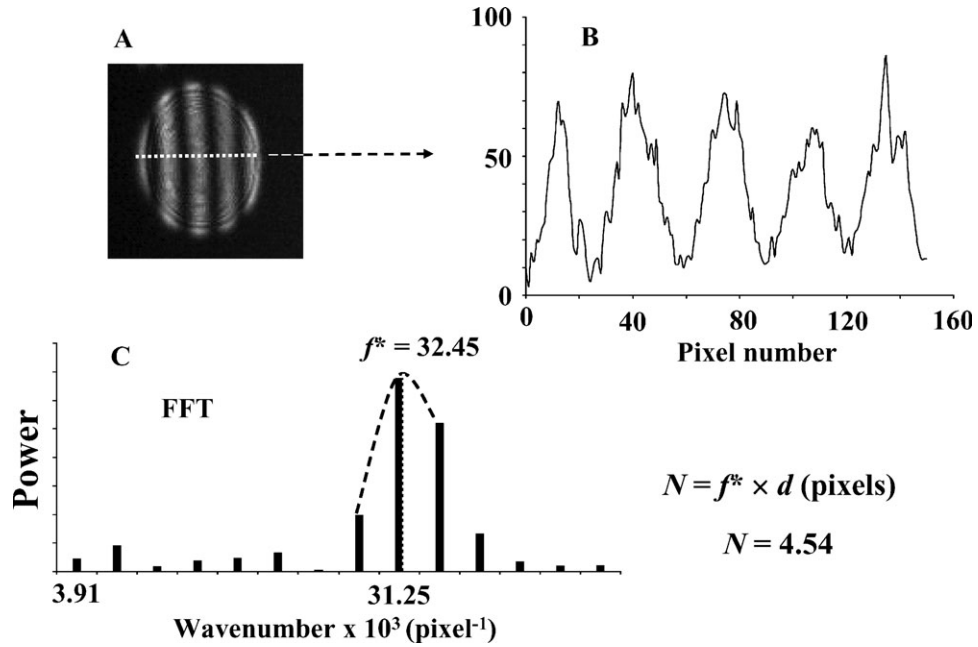

Fig. 4 Fringe counting: (A) an interferometric image of a droplet, (B) the horizontal intensity profile of the interference pattern, (C) fast Fourier transform and adjusted Gaussian fitting.

fringes) and velocities. Because of the large exposure time (50 μs) of the CCD camera, part of the background emission from the plasma is also recorded in the image.

3. Results and discussion

An important advantage of the current method over our previous PTV studies[23] in the ICP is the high accuracy in droplet pair identification and velocity calculations due to availability of two extra pieces of information, namely number of fringes and droplet image size. This is particularly advantageous in images that have more than one droplet (see Fig. 5). The center of each droplet image is calculated by finding the position of the edges of the droplet image from the intensity profiles (see Fig. 4). The measurement error for each edge position is estimated to be less than 5 pixels. For velocity calculations, two droplets must be considered, requiring the measurement of four edges. This leads to an error of less than 10 pixels in the distance traveled, translating to a velocity error of <1.4 m s^{-1} for a 45 μs double exposure image.

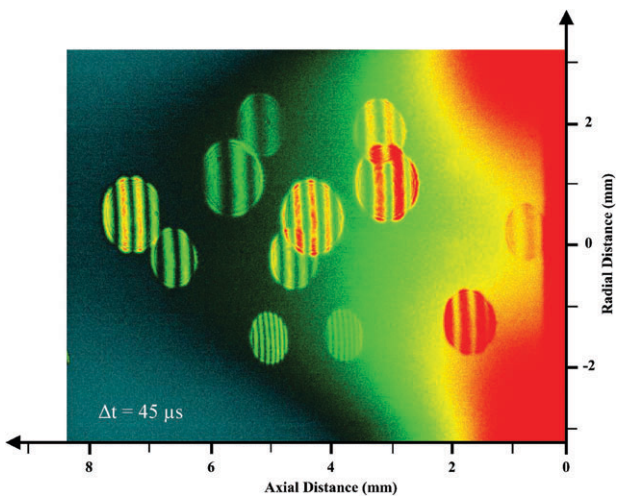

Fig. 5 Surviving droplet pairs in a typical double exposure (Δt = 45 μs) out-of-focus image. Scattering from the torch edge is captured on the right side of the image. Emission from the 1400 W Ar ICP is also observed at the center of the image. Colors are indicative of intensity at each pixel with red and blue for maximum and minimum intensities, respectively. The d-DIHEN is operated at 0.2 L min^{-1} gas flow and 85 μL min^{-1} solvent flow.

3.1. Effect of refractive index

As noted previously, the refractive index of water in air at 298 K is used in droplet size calculations. To estimate the error introduced by this value, the relative change in droplet diameter is calculated for a large range of refractive indices with respect to the reference value of n = 1.333. As illustrated in Fig. 6, an error of less than 1% is expected to arise due to the change in the refractive index once the droplets enter Ar ICP. Moreover, Fig. 6 illustrates that interferometric droplet imaging mainly responds to the size of the droplet rather than the optical properties of the solvent and consequently can be utilized for *in situ* study of the aerosol generated from solvents and mixtures when only an approximate knowledge is available about optical properties.

3.2. Size and velocity of the surviving droplets

The size–velocity correlations for 100 surviving droplets are shown in Fig. 7 at two nebulizer gas flow rates of 0.2 (Fig. 7A) and 0.15 L min^{-1} (Fig. 7B). A minimum velocity of about 20 m s^{-1} is observed for both conditions, indicating that the minimum droplet velocity in the ICP is mainly influenced by the gas velocity in analytical zone of the plasma. This velocity

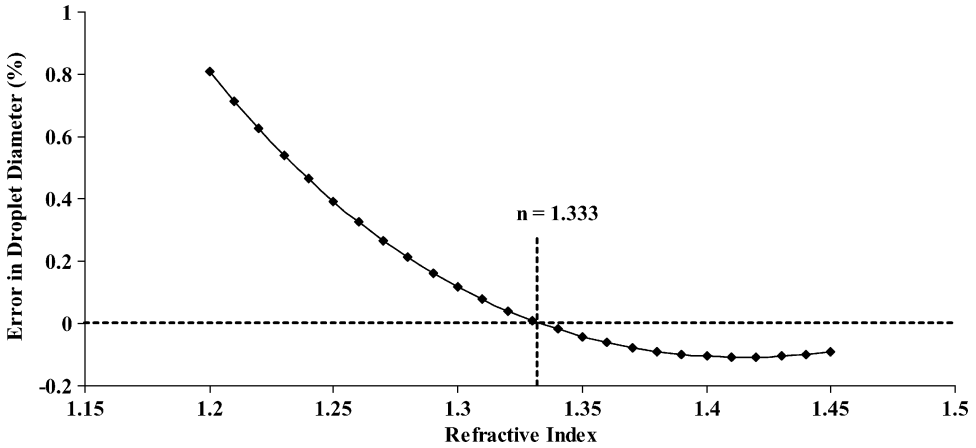

Fig. 6 Variation of the calculated droplet diameter due to change in refractive index with respect to the reference value of 1.333 (water in air at 298 K).

is dictated by thermal expansion of the plasma gas and is generally independent of the nebulizer gas flow rate.[41] However, the maximum velocity of surviving droplets exhibits a strong dependence on nebulizer gas flow rate, decreasing from 70 m s^{-1} (Fig. 7A) to 50 m s^{-1} (Fig. 7B) by lowering the nebulizer gas flow rate from 0.2 L min^{-1} to 0.15 L min^{-1}. This trend is in agreement with the droplet velocities measured for direct injection nebulizers in the absence of the plasma.[15]

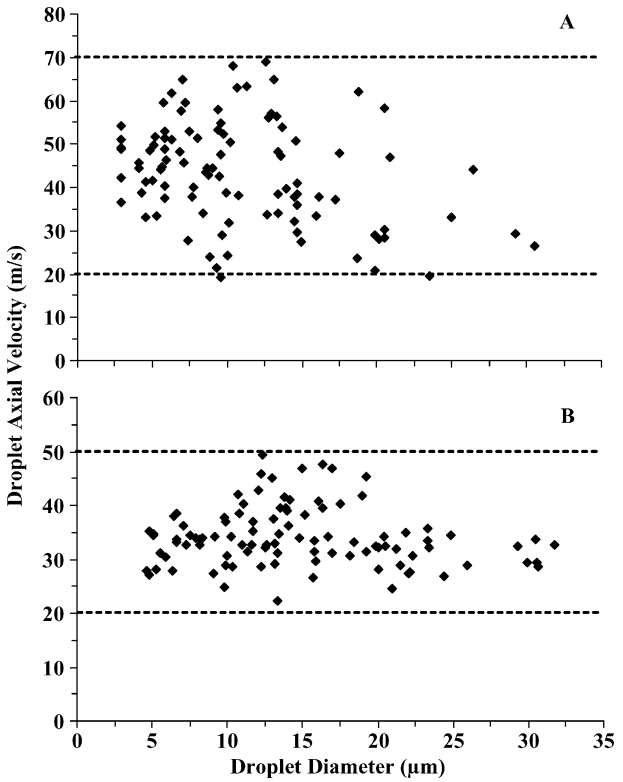

Fig. 7 Size–velocity correlation for 100 surviving droplets generated by d-DIHEN (85 μL min^{-1} solvent flow rate) in analytical zone of a 1400 W Ar ICP. (A) Nebulizer gas flow rate = 0.2 L min^{-1}. (B) Nebulizer gas flow rate = 0.15 L min^{-1}. Note that the view window is a rectangle of 8.4 mm × 6.4 mm placed at 7 mm downstream of the load coil at the center of the plasma.

The surviving droplets are generally smaller than 35 μm in diameter. At higher nebulizer gas flow rates (Fig. 7A), a larger number of smaller droplets (<10 μm) are observed in the analytical zone because of their higher velocities. Lower velocities are observed for droplets larger than 20 μm under both operating conditions, however, the size–velocity correlation is not very strong for smaller droplets (Fig. 7). This may be due to the limited number of counted droplets. Studies are underway in our laboratory for treating a large number of droplets, utilizing customized image processing softwares.

3.3. Droplet evaporation rates

Considering a precision of 5% in our droplet sizing method, a longer time interval compared to PTV studies above (Δt = 45 μs) must be used for accurate measurement of the droplet size change and the evaporation rates. An optimum Δt of 125 to 150 μs is experimentally determined for evaporation rate studies within our field of view (6.4 × 8.4 mm, and 7 mm downstream the load coil). Assuming droplet evaporation in ICP is heat transfer limited,[21,24,25,29] the evaporation rate (b) can be calculated using:

$$d_1^2 - d_2^2 = b\Delta t \qquad (7)$$

where d_1, and d_2 are initial and final droplet diameters, respectively. Also, for these experiments the d-DIHEN is operated at a gas flow rate of 0.15 L min^{-1} to produce slower droplets that can be followed during their evaporation. The data for four droplets is summarized in Table 2. Estimated errors in evaporation rates are calculated by error propagation using eqn (7). Note that the large Δt used for evaporation studies limits the range of droplet velocities to less than 40 m s^{-1}. Faster droplets do not result in a droplet pair in the area monitored with the current setup. Moreover, the larger distance between the droplet pairs introduces uncertainties in accurate identification of conjugate droplets.

The desolvation rates in Table 2 range from 0.26 to 0.36 mm^2 s^{-1} and are lower than the rate (0.54 mm^2 s^{-1})[29] calculated using a continuum evaporation model in a 3000 K Ar ICP. However, when the rarefaction factor for proximity of the droplet diameter and gas mean free path is taken into

Table 2 Evaporation rates of the droplets[a] in a 1400 W Ar ICP

	Initial diameter/μm	Final diameter/μm	Δt/μs	Velocity/ m s^{-1}	Evaporation rate[b]/mm^2 s^{-1}	Error in evaporation rate (%)
Droplet 1	7.6	4.0	150	36	0.28	14
Droplet 2	10.5	8.0	125	38	0.36	28
Droplet 3	8.3	6.0	125	37	0.26	24
Droplet 4	8.9	6.5	125	27	0.29	24

[a] Droplets are generated using a demountable-DIHEN at gas flow rate of 0.15 L min^{-1} and solution flow rate of 85 μL min^{-1}. [b] This rate is referred to as "rate of desolvation" in ref. 21 and "desolvation rate constant" in ref. 24.

account, the simulation result (0.43 mm^2 s^{-1})[29] approaches the experimental datum in this study. This suggests that the gas temperature around the desolvating droplet is about 3000 K with the current experimental setup. Higher temperatures (~5000 K) exist away from the droplet. Currently, there are no experimental data reported for the direct measurement of gas temperature around the droplet and only one desolvation model in ICP considers droplet–plasma interactions.[28] However, the operating parameters used in ref. 28 are dramatically different from the common conditions used in ICP spectrometries. In addition, an average effect of droplet evaporation on plasma gas temperature is calculated at steady state conditions in this model and individual droplet evaporation rates are not reported. Note that the evaporation rates for the d-DIHEN droplets in a 1400 W ICP occur in the range reported in previous studies (0.28 mm^2 s^{-1}, and 0.38 mm^2 s^{-1})[21,24] for droplets introduced by the MDMI into a 1000 W ICP. This proximity is attributed to the larger solvent load introduced into the 1400 W ICP using the d-DIHEN at 85 μL min^{-1} which results in reduced plasma gas temperature and decreased evaporation rate. Higher desolvation rates (up to 0.78 mm^2 s^{-1})[42–44] are reported for flames mainly due to the larger thermal conductivity of the flame gas constituents (mostly nitrogen with additives such as helium).

The data in Table 2 may be used to estimate the initial diameter of the droplets before introduction into the ICP. The initial droplet diameters must be smaller than 18 μm, assuming a travel distance of 3 cm (from the intermediate tube to 15 mm downstream the load coil) and a final droplet diameter of zero using eqn (7). This value, however, is an overestimation because the time required for the droplet to reach a steady-state is neglected in the calculations. In addition, a constant evaporation rate is assumed for this estimation which is questionable because the droplets pass through different temperature zones in the plasma. For complete desolvation of fast droplets (see Fig. 7A for droplets traveling faster than 50 m s^{-1}), a smaller initial diameter is required.

4. Conclusions and future directions

Interferometric droplet imaging (IDI) is used to measure size, velocity, and evaporation rate of droplets inside an Ar ICP. The imaging technique introduced in this report has several advantages over previously used methods: (1) a large area of the plasma is monitored as opposed to point measurements using a phase Doppler particle analyzer, (2) the method is fairly insensitive to laser light intensity fluctuations because an interference pattern is collected rather than measuring absolute intensity, (3) variation of refractive index has negligible effect on droplet sizing, leading to an improved droplet monitoring approach in the environments where the exact optical properties are not known, and (4) size, velocity, and evaporation rate of the droplets can be measured simultaneously for correlation studies.

The results indicate that at normal operating conditions for direct injection nebulizers (for example for a d-DIHEN operated at 0.2 L min^{-1} of gas flow rate and 85 μL min^{-1} of solution flow rate) surviving droplets in the analytical zone of the plasma possess diameters and velocities of 3–30 μm and 20–70 m s^{-1}, respectively. Evaporation rates of 0.26–0.36 mm^2 s^{-1} are measured for individual droplets which are in good agreement with results of our computer based simulations, within the limitations of each approach, for an argon environment at 3000 K. Based on the measured droplet evaporation rate and velocity, the maximum estimated initial diameter is 18 μm for complete evaporation.

The current instrumental setup is limited in terms of precision of droplet sizing and consequently the precision of measured evaporation rates. Studies are underway to improve the measurement precision which will allow the collection and analysis of correlated size, velocity, and evaporation rates for a large range of droplet properties. In addition, other sample introduction systems will be considered in future studies.

Acknowledgements

This research was sponsored by the Department of Energy (DE-FG02-93ER14320). We express our gratitude to Perkin Elmer Corporation for the gift of Elan 5000 generator. We thank Dr Callum Gray of LaVision Inc., for the loan of Macro-Planar lens. Special thanks to Mr William Rutkowski of George Washington University for his excellent machine shop services. The constructive discussions with Mr Kavous Jorabchi of State University of New York at Stony Brook are greatly appreciated.

References

1 *Inductively Coupled Plasma Mass Spectrometry*, ed. A. Montaser, VCH-Wiley, New York, 1998.
2 *Inductively Coupled Plasmas in Analytical Atomic Spectrometry*, ed. A. Montaser and D. W. Golightly, Wiley-VCH, New York, 2nd edn, 1992.
3 A. Montaser, M. G. Minnich, J. A. McLean, H. Liu, J. A. Caruso and C. W. McLeod, Sample introduction in ICPMS, in *Inductively*

Coupled Plasma Mass Spectrometry, ed. A. Montaser, Wiley-VCH, New York, USA, 1998, pp. 83–264.
4 A. Montaser, M. G. Minnich, H. Liu, A. G. T. Gustavson and R. F. Browner, Fundamental aspects of sample introduction in ICP spectrometry, in *Inductively Coupled Plasma Mass Spectrometry*, ed. A. Montaser, Wiley-VCH, New York, USA, 1998, pp. 335–420.
5 J. A. McLean, M. G. Minnich, L. A. Iacone, H. Liu and A. Montaser, Nebulizer diagnostics: fundamental parameters challenges and techniques on horizon, *J. Anal. At. Spectrom.*, 1998, **13**, 829–842.
6 N. Mohamed, R. C. Fry and D. L. Wetzel, Laser Fraunhofer diffraction studies of aerosol droplet size in atomic spectrochemical analysis, *Anal. Chem.*, 1981, **53**, 639–645.
7 R. H. Clifford, I. Ishii, A. Montaser and G. A. Meyer, Dual-beam, light-scattering interferometry for simultaneous measurements of droplet-size and velocity distributions of aerosols from commonly used nebulizers, *Anal. Chem.*, 1990, **62**, 390–394.
8 S. C. K. Shum, S. K. Johnson, H.-M. Pang and R. S. Houk, Spatially resolved measurements of size and velocity distributions of aerosol droplets from a direct injection nebulizer, *Appl. Spectrosc.*, 1993, **47**, 575–583.
9 A. Montaser and H. Liu, Phase-Doppler diagnostic studies of primary and tertiary aerosols produced by a high-efficiency nebulizer, *Anal. Chem.*, 1994, **66**, 3233–3242.
10 J. W. Olesik and L. C. Bates, Characterization of aerosols produced by pneumatic nebulizers for inductively coupled plasma sample introduction: Effect of liquid and gas flow rates on volume based drop size distributions, *Spectrochim. Acta*, 1995, **50B**, 285–303.
11 J. L. Todoli, A. Canals and V. Hernandis, Behavior of a single-bore high-pressure pneumatic nebulizer operating with alcohols in inductively coupled plasma atomic emission spectrometry, *J. Anal. At. Spectrom.*, 1997, **12**, 391.
12 J. A. McLean, R. A. Huff and A. Montaser, Fundamental properties of aerosol produced in helium by a direct injection nebulizer, *Appl. Spectrosc.*, 1999, **53**, 1331–1339.
13 J. A. McLean, M. G. Minnich, A. Montaser, J. Su and W. Lai, Optical patternation: a technique for three-dimensional aerosol diagnostics, *Anal. Chem.*, 2000, **72**, 4796–4804.
14 M. G. Minnich, J. A. McLean and A. Montaser, Spatial aerosol characteristics of a direct injection high efficiency nebulizer *via* optical patternation, *Spectrochim. Acta*, 2001, **56B**, 1113–1126.
15 K. Kahen, K. Jorabchi, C. Gray and A. Montaser, Spatial mapping of droplet velocity and size in direct and indirect nebulization, *Anal. Chem.*, 2004, **76**, 7194–7201.
16 J. W. Olesik and J. C. Fister III, Incompletely desolvated droplets in argon inductively coupled plasmas: Their number, original size and effect on emission intensities, *Spectrochim. Acta*, 1991, **46B**, 851–868.
17 S. E. Hobbs and J. W. Olesik, Inductively coupled plasma mass spectrometry signal fluctuations due to individual aerosol droplets and vaporizing particles, *Anal. Chem.*, 1992, **64**, 274–83.
18 S. E. Hobbs and J. W. Olesik, The effect of desolvating aerosol and vaporizing particles on ionization and excitation in Ar inductively coupled plasma, *Spectrochim. Acta*, 1993, **48B**, 817–833.
19 J. W. Olesik, Investigating the fate of individual sample droplets in inductively coupled plasmas, *Appl. Spectrosc.*, 1997, **51**, 158A–175A.
20 R. S. Houk, R. K. Winge and X. Chen, High speed photographic study of wet droplets and solid particles in the inductively coupled plasma, *J. Anal. At. Spectrom.*, 1997, **12**, 1139–1148.
21 A. Lazar and P. B. Farnsworth, Matrix effect studies in inductively coupled plasmas with monodisperse droplets. Part I: the influence of matrix on the vertical analyte emission profile, *Appl. Spectrosc.*, 1999, **53**, 457–464.
22 D. B. Aeschliman, S. J. Bajic, D. P. Baldwin and R. S. Houk, High-speed digital photographic study of an inductively coupled plasma during laser ablation: comparison of dried solution aerosols from a microconcentric nebulizer and solid particles from laser ablation, *J. Anal. At. Spectrom.*, 2003, **18**, 1008–1014.
23 K. Jorabchi, K. Kahen, C. Gray, Callum and A. Montaser, *In situ* visualization and characterization of aerosol droplets in an inductively coupled plasma, *Anal. Chem.*, 2005, **77**, 1253–1260.
24 J. A. Kinzer and J. W. Olesik, Measurement of droplet desolvation in an inductively coupled plasma using phase Doppler particle analysis and Mie scattering resonances, *Spectrochim. Acta B*, 2005, submitted.
25 C. M. Benson, S. F. Gimelshein, D. A. Levin and A. Montaser, Simulation of droplet heating and desolvation in an inductively coupled plasma—Part I, *Spectrochim. Acta*, 2001, **56B**, 1097–1112.
26 J. A. Horner, S. A. Lehn and G. M. Hieftje, Computerized simulation of aerosol–droplet desolvation in an inductively coupled plasma, *Spectrochim. Acta*, 2002, **57B**, 1025–1042.
27 C. M. Benson, J. Zhong, S. F. Gimelshein, D. A. Levin and A. Montaser, Simulation of droplet heating and desolvation in an inductively coupled plasma—Part II coalescence in the plasma, *Spectrochim. Acta*, 2003, **58B**, 1453–1471.
28 Y. Shan and J. Mostaghimi, Numerical simulation of aerosol droplets desolvation in a radio frequency inductively coupled plasma, *Spectrochim. Acta*, 2003, **58B**, 1959–1977.
29 C. M. Benson, D. A. Levine, J. Zhong, S. F. Gimelshein and A. Montaser, Kinetic model for aerosol droplets in high-temperature environments, *J. Thermophys. Heat Transfer*, 2004, **18**, 122–134.
30 A. R. Glover, S. M. Skippon and R. D. Boyle, Interferometric laser imaging for droplet sizing: a method for droplet size measurements in sparse systems, *Appl. Opt.*, 1995, **34**, 8409–8421.
31 M. Golombok, V. Morin and C. Mouniam-Rouselle, droplet diameter and interference fringes between reflected and refracted light, *J. Phys. D: Appl. Phys.*, 1998, **D31**, L59–L62.
32 M. Maeda, T. Kawaguchi and K. Hishida, Novel interferometric measurement of size and velocity distributions of spherical particles in fluid flows, *Meas. Sci. Technol.*, 2000, **11**, L13–L18.
33 M. Maeda, Y. Akasaka and T. Kawaguchi, Improvements of the interferometric technique for simultaneous measurement of droplet size and velocity vector field and its application to a transient spray, *Exp. Fluids*, 2002, **33**, 125–134.
34 T. Kawaguchi, Y. Akasaka and M. Maeda, Size measurements of droplets and bubbles by advanced interferometric laser imaging technique, *Meas. Sci. Technol.*, 2002, **13**, 308–316.
35 J. Massen, J. Harbo, T. I. Nonn, D. Blondel, B. H. Hjertager and T. Solberg, Measurement of droplet size and velocity distributions in sprays using interferometric particle imaging and particle tracking velocimetry, presented at *The International Conference on Liquid Atomization and Spray Systems*, Italy, July, 2003, pp. 13–17.
36 N. Fujisawa, A. Hosokawa and S. Tomimatsu, Simultaneous measurement of droplet size and velocity field by an interferometric imaging technique in spray combustion, *Meas. Sci. Technol.*, 2003, **14**, 1341–1349.
37 A. Graßmann and F. Peters, Size measurement of very small spherical particles by Mie scattering imaging, *Part. Part. Syst. Charact.*, 2004, **21**, 379–389.
38 C. S. Westphal, K. Kahen, W. F. Rutkowski, B. W. Acon and A. Montaser, Demountable direct injection high efficiency nebulizer for inductively coupled plasma mass spectrometry, *Spectrochim. Acta, Part B*, 2004, **59B**, 353–368.
39 J. L. Todoli and J.-M. Mermet, Evaluation of a direct injection high-efficiency nebulizer (DIHEN) by comparison with a high-efficiency nebulizer (HEN) coupled to a cyclonicspray chamber as a liquid sample introduction system for ICP-AES, *J. Anal. At. Spectrom.*, 2001, **16**, 514–520.
40 S. E. O'Brien, J. R. Chirinos, K. Jorabchi, K. Kahen, M. E. Cree and A. Montaser, Investigation of the direct injection high efficiency nebulizer for axially and radially viewed inductively coupled plasma atomic emission spectrometry, *J. Anal. At. Spectrom.*, 2003, **18**, 910–916.
41 M. T. Cicerone and P. B. Farnsworth, A simple non-invasive method for the measurement of gas velocities in an inductively coupled plasma, *Spectrochim. Acta, Part B*, 1989, **44B**, 897–907.
42 G. M. Hieftje and H. V. Malmstadt, Unique system for studying flame spectrometric processes, *Anal. Chem.*, 1968, **40**, 1860–1867.
43 N. C. Clampitt and G. M. Hieftje, Mechanism of desolvation of sample droplets in flame spectrometry, *Anal. Chem.*, 1972, **44**, 1211–1218.
44 N. C. Clampitt and G. M. Hieftje, Influence of flame gas thermal conductivity on atom formation in flame spectrometry, *Anal. Chem.*, 1974, **46**, 382–386.

